

Dynamic energy transfer in non-covalently functionalized reduced graphene oxide/silver nanoparticle hybrid (NF-RGO/Ag) with NF-RGO as the donor material

El Hadji Mamour Sakho^{1,2} · Oluwatobi S. Oluwafemi^{3,4} · Sabu Thomas^{2,5} · Nandakumar Kalarikkal^{1,2}

Received: 9 July 2016 / Accepted: 6 October 2016 / Published online: 12 October 2016
© Springer Science+Business Media New York 2016

Abstract Non-covalent functionalization of reduced graphene oxide has been shown to stabilize its dispersion and solubility in different solvents without destruction on the graphene sheet network. We herein report a simple and efficient strategy for the preparation of non-covalently functionalized reduced graphene oxide/silver nanoparticle hybrid (NF-RGO/Ag) in which non-covalently functionalized reduced graphene oxide (NF-RGO) acted as donor material. Graphite oxide functionalized with 1-pyrenecarboxylic acid and silver nitrate (AgNO_3) were reduced by hydrazine hydrate to produce NF-RGO/Ag hybrid. The structure and morphology of NF-RGO and NF-RGO/Ag hybrid were respectively characterized by FTIR spectroscopy, UV–Vis spectroscopy, Raman spectroscopy, XRD, EDAX and TEM while the luminescence properties were studied using photoluminescence spectroscopy and time domain fluorescence spectroscopy. The luminescence

spectroscopy revealed that the photoluminescence quenching observed in the NF-RGO/Ag hybrid is due to an unusual dynamic energy transfer from NF-RGO to silver nanoparticles (Ag-NPs). This finding leads to a better understanding of photoluminescence quenching of NR-RGO by Ag-NPs and suggests that NF-RGO/Ag hybrid has great potential in various applications such as solar cells, water splitter, photothermal and photochemical applications.

1 Introduction

Graphene, a 2D nano-carbon atoms arranged in honeycomb lattice has attracted tremendous attentions since its first isolation from bulk graphite [1–3]. This is due to its fascinating properties which includes excellent electron mobility, good conductivity, good thermal and chemical stability, high thermal conductivity and remarkable mechanical strength [1, 4, 5]. Because of these properties, it has been shown to be an excellent electron or energy transport materials for various applications such as solar cells, sensors, photochemical and photothermal applications [6].

Various synthetic routes, such as mechanical exfoliation, chemical vapor deposition (epitaxial growth) and chemical solution method have been reported for the synthesis of high quality graphene [7, 8]. Among these, the chemical oxidation of graphite to form graphene oxide (GO) and its subsequent reduction to graphene has proved to be the most promising method. This is due to its, simplicity, cost-effectiveness and high yield. During reduction of graphene oxide, the major oxygen containing group of the resulting RGO are removed, which may limit its application. Functionalization of RGO is important in

✉ Oluwatobi S. Oluwafemi
oluwafemi.oluwatobi@gmail.com

✉ Nandakumar Kalarikkal
nkkalarikkal@mgu.ac.in

¹ School of Pure and Applied Physics, Mahatma Gandhi University, Kottayam, Kerala 686560, India

² International and Inter University Centre for Nanoscience and Nanotechnology, Mahatma Gandhi University, Kottayam, Kerala 686560, India

³ Department of Applied Chemistry, University of Johannesburg, P.O. Box 17011, Doornfontein, Johannesburg 2028, South Africa

⁴ Centre for Nanomaterials Sciences Research, University of Johannesburg, Johannesburg, South Africa

⁵ School of Chemical Science, Mahatma Gandhi University, Kottayam, Kerala 686560, India

making RGO reach desired properties and improve its applications. Functionalizing RGO will improve its solubility in several organic and inorganic solvents, increase the manipulation and processing capability of RGO for device fabrication and increase the ability of RGO to disperse in matrices or load nanomaterials [9]. An et al. [10] reported the synthesis of stable aqueous dispersions of graphene by non-covalent functionalization of graphene with 1-pyrenecarboxylic acid (1-PCA). In this work, graphite was directly exfoliated into aqueous dispersions of single, few, and multilayered graphene flakes by a non-covalent functionalization of graphene with PCA in a media such as water, methanol and ethanol through non-destructive π - π interaction. In another development, Chen et al. [11] reported transfer of energy from CdSe/ZnS nanocrystals to a single graphene layer. Supur et al. [12] prepared perylenediimide-graphene oxide hybrid which showed an electron transfer phenomenon from perylenediimide to graphene. Jiang et al. [13] investigated the electron transfer from heteropoly blue to graphene oxide for the synthesis of graphene. All these works involved the use of graphene as an acceptor while only few reports focused on graphene oxide as a donor material [14, 15].

Reduced graphene oxide coated with Ag-NPs has attracted enormous interest because of its unique optoelectronic properties as well as its high catalytic activity [16, 17]. Tang et al. [18] in order to prepare graphene-Ag nanocomposites, simultaneously reduced graphene oxide and silver ion with formaldehyde. Yola et al. [19] functionalized graphene oxide with 2-aminoethanethiol (2-AET) and attached Ag-NPs on the surfaces of the as-functionalized graphene oxide. Mehl et al. [20] prepared thin and transparent films of graphene/Ag-NPs by liquid-liquid interfaces. Though these methods involved the use of graphene oxide as a donor in which, the graphene oxide were covalently functionalized. The hydrophobic nature of graphitic materials coupled with the relatively stable interlayer adhesion of graphite make it difficult to directly exfoliate it into graphene [10], thus, there is a need to develop an efficient method to non-covalently functionalize graphene. Non-covalent functionalization stabilizes high concentrations of graphene sheets in aqueous dispersions and has less effect on the structure as well as properties of graphene sheets [10]. Therefore, in this work we describe a novel, simple and significant way to non-covalently functionalize reduced graphene oxide. The functionalized reduced graphene oxide (NF-RGO) was decorated with silver nanoparticles and the photophysical properties of the NF-RGO/Ag-NPs hybrid were investigated. The mechanism of photoluminescence quenching of NF-RGO by Ag-NPs through a combination of spectroscopic studies was also reported.

2 Experimental section

2.1 Materials and methods

1-Pyrenecarboxylic acid (1-PCA), silver nitrate (AgNO_3) and graphite powder were purchased from Sigma-Aldrich. Concentrated sulfuric acid [H_2SO_4 (98 %)], potassium permanganate (KMnO_4), sodium nitrate (NaNO_3), hydrogen peroxide (H_2O_2 , 30 %), and hydrazine hydrate were purchased from Merck. All chemicals were used as received.

2.2 Synthesis of graphite oxide (GO)

Graphite oxide was synthesized by oxidation of graphite according to Hummer's method with slight modifications [21, 22]. In a typical reaction, 69 ml of H_2SO_4 was cooled to 0 °C and after 45 min of cooling, it was added to a mixture of graphite flakes (3.0 g) and NaNO_3 (1.5 g). The mixture was again kept in the ice bath (0 °C). KMnO_4 (9.0 g) was slowly added to keep the reaction below 20 °C. The reaction was heated to 35 °C and stirred for 30 min followed by slow addition of double distilled water (138 ml) to increase the temperature to 95 °C. The reaction was heated at 95 °C for 15 min, after which the heat was removed. The reaction was cooled down using ice bath for 10 min. 420 ml of double distilled water and 30 ml of H_2O_2 were added in order to terminate the reaction. The solution was allowed to settle down overnight and washed with double distilled water several times until the pH became neutral through settling and decantation process. The solution was filtered with Whatman filter paper. The filtrate was collected and vacuum-dried at 60 °C for one night to finally get graphite oxide (GO).

2.3 Preparation of non-covalent functionalized reduced graphene oxide/silver nanoparticle hybrid (NF-RGO/Ag)

Solution of 1-pyrenecarboxylic acid with pH 11.2 was prepared in double distilled water by adding 1 M solution of NaOH to 0.04 g of 1-pyrenecarboxylic acid. The resulting solution was added into 300 ml aqueous solution of GO. The mixture was sonicated for 45 min and 2 ml aqueous solution of silver nitrate was added and kept under sonication for another 15 min. After the solution was removed from probe sonicator, it was mixed with 300 μl of hydrazine and heated at 80 °C for 24 h to allow simultaneous reduction of graphene oxide and Ag to NF-RGO/Ag. The experiment was repeated using different concentrations of AgNO_3 (0.1, 0.3, 0.5 and 1 M) and the products were designated as NR-RGO/Ag (xM) where x is the concentration of AgNO_3 . Non-covalent functionalized

reduced graphene oxide (NF-RGO) alone was obtained by following the same procedure in the absence of AgNO_3 solution.

2.4 Characterizations

X-ray diffraction (XRD) patterns were recorded on a Philips X'Pert Pro powder diffractometer with $\text{Cu K}\alpha$ radiation (1.54056 Å). Fourier transform infrared (FTIR) analysis was performed with Perkin Elmer FTIR spectrometer. Morphologies of the samples were examined using transmission electron microscopy (TEM, JEOL JEM 2100). Specimens for both TEM and EDAX were prepared by dispersing the samples in double distilled water. Then, a few of the dispersing solutions were drop-casted on carbon-coated copper grids. The absorption spectrum was taken using UV–Vis spectrophotometer (SHIMADZU, UV-2450). Raman spectra were recorded using Horiba Jobin–Yvon LabRAM Micro Raman spectrometer with Argon ion laser, with 514.5 nm as excitation wavelength. Photoluminescence spectra were recorded using a Horiba Jobin–Yvon Ltd fluoromax-4 Spectrofluorometer. The picosecond (ps) PL lifetimes were measured by the TCSPC technique (Horiba Jobin–Yvon IBH limited decay analysis software) with 2 exponentials decay components. The light source used was a NanoLED (Horiba Jobin–Yvon) of wavelength 340 nm.

3 Results and discussion

3.1 X-rays diffraction (XRD) analysis

XRD patterns of the graphite (G), GO, NF-RGO and NF-RGO/Ag hybrid with different concentration of AgNO_3

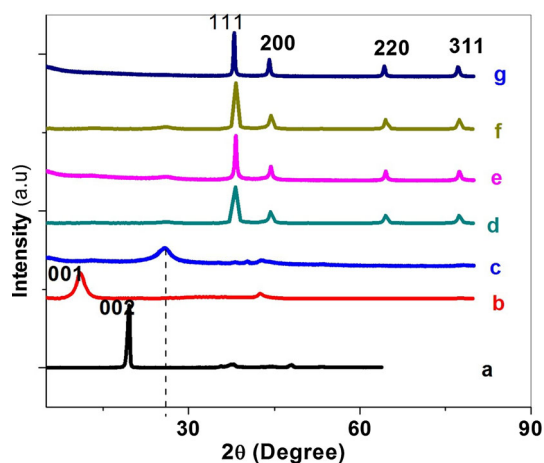


Fig. 1 XRD patterns of (a) G, (b) GO, (c) NF-RGO and NF-RGO/Ag hybrid at various concentrations of AgNO_3 , (d) 0.1 M, (e) 0.3 M, (f) 0.5 M and (g) 1 M, respectively

solution are shown in Fig. 1a–g. XRD pattern of G (Fig. 1a) exhibits a very sharp characteristic peak at 26.36° corresponding to (002) plane with an interlayer d -spacing of 3.35 Å. This also highlights the good crystallinity of this material (JCPDS card No. 41-1487). After oxidation, the native peak of graphite powder at 26.36° disappeared and a new diffraction peak appeared at 10.94° corresponding to (001) plane with an interlayer d -spacing of 8.09 Å (Fig. 1b) which indicates the formation of graphite oxide. The increase in d -spacing observed between G and GO confirmed that graphite, a building block of graphene sheet was slightly exfoliated [23]. Figure 1c shows the XRD pattern of the NF-RGO. The spectra exhibits a broad diffraction peak at 25.80° indicating that NF-RGO in the absence of Ag-NPs was reduced to a few layers of NF-RGO by using hydrazine hydrate as reducing agent [24]. Figure 1d–g show the XRD patterns of NF-RGO/Ag with different molar concentrations of AgNO_3 solution; 0.1, 0.3, 0.5 and 1 M, respectively. The main peaks at 38.13° , 44.30° , 64.50° , and 77.80° were attributed respectively to the (111), (200), (220), and (311) crystallographic planes of the face centered cubic (FCC) of Ag nanoparticle [JCPDS card No. 07-0783]. All the NF-RGO/Ag at different concentrations of AgNO_3 solution exhibit the same diffraction patterns. On the other hand, the peak at 10.94° disappeared for all the NF-RGO/Ag hybrids at different concentrations. This suggest that the regular layered structure NF-RGO was totally exfoliated after insertion of Ag-NPs. This could be attributed to the insertion and distribution of small Ag-NPs and the attachment of 1-pyrenecarboxylic acid (1-PCA) functional groups on NF-RGO surface. 1-PCA act like a stabilizer and prevent restacking of the layers on the structure of NF-RGO [23–28].

3.2 UV–visible spectroscopy

UV–Vis spectroscopy was used to study the electronic properties of GO, NF-RGO and NF-RGO/Ag (xM) and also to monitor the formation of Ag-NPs on NF-RGO. Figure 2a–c shows the UV–Vis spectra of GO, NF-RGO and NF-RGO/Ag hybrid with 0.3 M of AgNO_3 solution, respectively. The characteristic peaks of GO at 232 and a shoulder at 300 nm were attributed to the π – π^* transition of aromatic C–C bonds and n – π^* transitions of C=O bonds respectively [23, 24]. The red shift in the GO main peak position from 232 to 243 nm and the disappearance of the shoulder at 300 nm for both NF-RGO and NF-RGO/Ag with 0.3 M of AgNO_3 solution indicates that extensive conjugated sp^2 -carbon network of GO is restored in both NF-RGO and NF-RGO/Ag hybrid. In addition, the presence of Ag-NPs on the surface of NF-RGO is justified by the appearance of surface plasmon resonance (SPR) absorption band of Ag-NPs at 404 nm. In Fig. 2b, the sharp

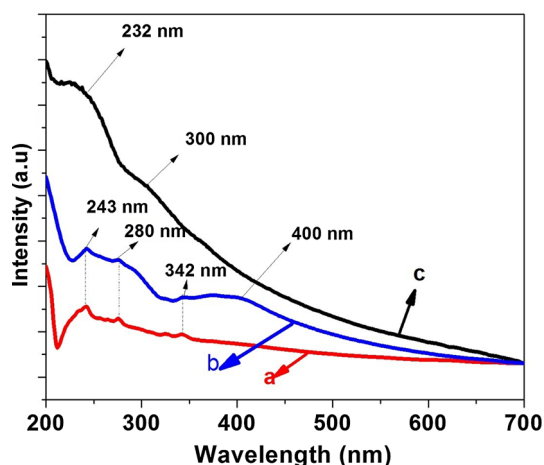


Fig. 2 UV-Vis absorption spectra of (a) NF-RGO, (b) NF-RGO/Ag at 0.3 M of AgNO_3 and (c) GO

absorption peaks observed at 280 and 342 nm confirmed the non-covalent functionalization of PCA on the surface of RGO. This might be attributed to the fact that, the PCA, a well-known polyaromatic derivative absorb a great amount of UV light when exposed to UV region. It has also been found that PCA retains its intrinsic useful property, when bonded with RGO [28]. Furthermore, the intensity at 280 nm and 342 nm peak positions attributed to PCA decrease in NF-RGO/Ag (xM), suggesting that $-\text{COOH}$ groups of PCA provide sites for hydrogen bonding with silver nanoparticle. Figure 3a–c shows the UV-Vis spectra of NF-RGO/Ag hybrid at 0.1, 1 and 0.5 M concentrations of AgNO_3 solution. The spectra show that, the surface plasmon resonance (SPR) absorption band of Ag-NPs disappeared when 0.1 M (Fig. 3a) and 1 M (Fig. 3b) of AgNO_3 were used. This might be assigned to the low Ag-NPs concentration at 0.1 M hence, no reduction reaction.

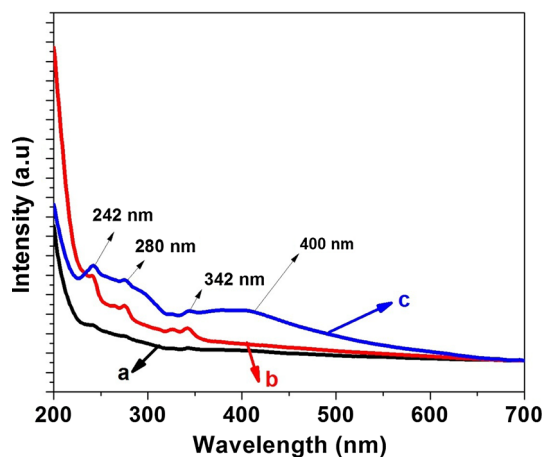


Fig. 3 UV-Vis absorption spectra of NF-RGO/Ag hybrid at various concentrations of AgNO_3 , (a) 0.1 M, (b) 1 M and (c) 0.5 M, respectively

At high concentration of 1 M, the rate of reduction is very slow due to insufficient reductant present in the solution.

3.3 FT-IR analysis

The FTIR spectra of GO, NF-RGO, and NF-RGO/Ag with various concentrations of AgNO_3 solution are shown in Figs. 4 and 5. The FTIR spectrum of GO (Fig. 4a) show peaks at 3251 , 1706 , 1619 , 1350 , 1207 and 1040 cm^{-1} which are assigned to the O–H stretching vibrations, C–O stretching of COOH groups, aromatic C=C bonds, O–H deformations of the C–OH, epoxy symmetrical ring deformation vibrations and C–O stretching vibrations, respectively [29]. After functionalization with PCA, the peak intensity at 1706 , 1350 , 1207 and 1040 cm^{-1} become reduced (Fig. 4b). This has been attributed to the chemical exfoliation and chemical reduction of GO. Furthermore, a new absorption peak attributed to the graphene sheet appears at 1506 cm^{-1} [30]. The results indicates that GO has been successfully non-covalently functionalized and reduced to NF-RGO. The FTIR spectra of NF-RGO/Ag at different concentration of AgNO_3 (Fig. 5) are similar to NF-RGO spectrum (Fig. 4b) but with lower band intensity. This decrease in the intensity, in addition with UV-Vis-analysis confirmed the bonding of Ag nanoparticles on the surface of NF-RGO to give NF-RGO/Ag hybrid.

3.4 Raman analysis

The Raman spectrum of GO (Fig. 6a) shows two main peaks at 1357 cm^{-1} (D band) and at 1570 cm^{-1} (G band) which are usually attributed to the doubly resonant disorder-induced mode and E_{2g} phonon of sp^2 carbon atoms, respectively [31]. The prominent D peak was from the structural defects created by the attachment of hydroxyl and epoxy groups on the carbon basal plane during acid

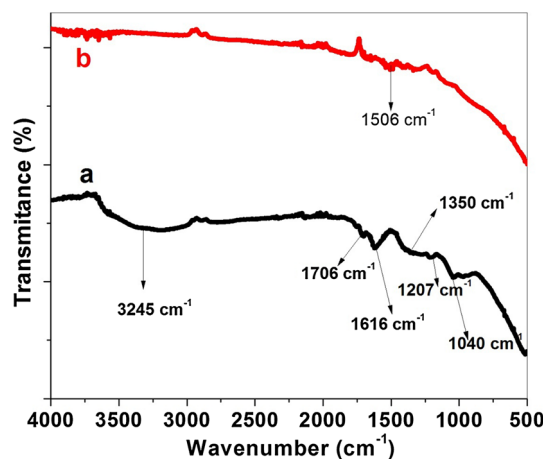


Fig. 4 FT-IR spectra of (a) GO and (b) NF-RGO

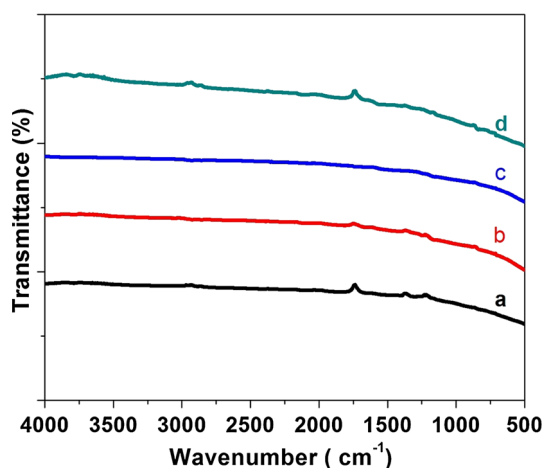


Fig. 5 FT-IR spectra of NF-RGO/Ag hybrid at various concentrations of AgNO_3 solution, (a) 0.1 M, (b) 0.3 M, (c) 0.5 M and (d) 1 M, respectively

oxidation of graphite flakes. In order to characterize the level of disorder in GO, NF-RGO and NF-RGO/Ag hybrid, we adopted the conventional method where the ratio of intensities of the D and G bands (I_D/I_G) of each sample was calculated. Since all NF-RGO/Ag hybrids exhibit similar Raman spectra, only the spectrum corresponding to 0.1 M hybrid system is shown. The I_D/I_G ratio of NF-RGO (Fig. 6b) increased to 1.25 compared to 0.98 for GO. This change indicates a decrease in the size of the in-plane sp^2 domains and partial ordered crystal structure of graphene due to the non-covalent functionalization. Furthermore, the D band and G band of NF-RGO shift from 1338 to 1357 and 1581 to 1570 cm^{-1} , respectively in comparison to GO. This further demonstrates that GO was successfully reduced during preparation of NF-RGO. In addition, the I_D/I_G ratio decrease from 1.25 for NF-RGO to 1.08 for NF-RGO/Ag hybrid. This change suggests that, the presence of

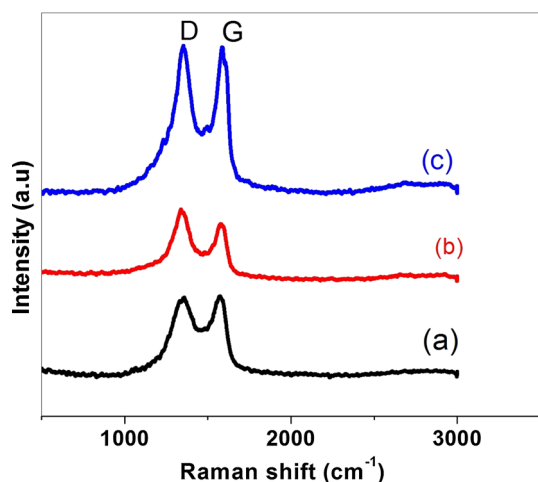


Fig. 6 Raman spectra of (a) GO, (b) NF-RGO and (c) NR-RGO/Ag hybrid (0.1 M)

Ag-NPs increases the size of the in-plane sp^2 domains of NF-RGO [32]. The G band of NF-RGO/Ag also shift from 1586 to 1570 cm^{-1} in comparison to GO, which indicates successful reduction of GO during the preparation of NF-RGO/Ag hybrid. Furthermore, the peak intensities of the D and G bands in NF-RGO/Ag hybrid (Fig. 6c) sample are significantly increased. This has been attributed to the surface enhanced Raman scattering (SERS) of Ag-NPs [33].

3.5 TEM and EDAX analysis

TEM images of NF-RGO/Ag composite (Fig. 7) show that Ag-NPs are spherical in shape and are well distributed on the surface of NF-RGO. At 0.1 M concentration of AgNO_3 solution (Fig. 7A1), the as-synthesized Ag-NPs are within the range of 8 and 23 nm with average particle diameter of 16.02 ± 7.50 nm. Increasing the concentration of AgNO_3 solution to 0.3 M (Fig. 7A2) produced particle in the range of 19–45 nm with an average particle diameter of 28.21 ± 8.76 nm. The TEM analyses show that increasing the concentration of AgNO_3 , caused increased in the particle size of the as-synthesized Ag-NPs. The typical HRTEM image of the NF-RGO/Ag hybrid at 0.1 M concentration of AgNO_3 solution (Fig. 7B1), shows the presence of lattice fringes demonstrating the high crystallinity of the as-synthesized Ag-NPs. The measured lattice spacing of 0.23 nm corresponds to the (111) crystal plane of face centered cubic (fcc) Ag. This is consistent with the d -spacing values reported in the XRD data (JCPDS card No. 04-0783). The presence of distinct rings in the selected area electron diffraction (SAED) patterns (Fig. 7B3) further showed the crystallinity of the as-synthesized Ag-NPs. At concentration of 0.5 M of AgNO_3 solution, the TEM micrograph (Fig. 7A3) shows the presence of bigger particles. The formation of bigger particle has been attributed to both aggregation and Ostwald ripening process [34]. At very high concentration of 1 M AgNO_3 solution (Fig. 7A4), significant aggregation of Ag-NPs was observed in the TEM micrograph. The TEM micrograph of NF-RGO (Fig. 7B4) shows the presence of two-dimensional structure consisting of sheets with micrometer long wrinkles. The presence of Ag-NPs in NF-RGO/Ag hybrid was confirmed by the energy-dispersive X-ray spectroscopy (EDAX). As shown in Fig. 9, EDAX of NF-RGO/Ag samples reveal the presence of Ag in NF-RGO/Ag hybrid. The intensity of the Ag peak increase with increase in the concentration of AgNO_3 solution. Furthermore, the EDAX data reveals a decrease in oxygen content as the AgNO_3 concentration increased. This suggests that the presence of Ag-NPs improved the structural restoration of GO. The EDAX data also displays the presence of other elements such as C and Cu. The C signal was mainly from

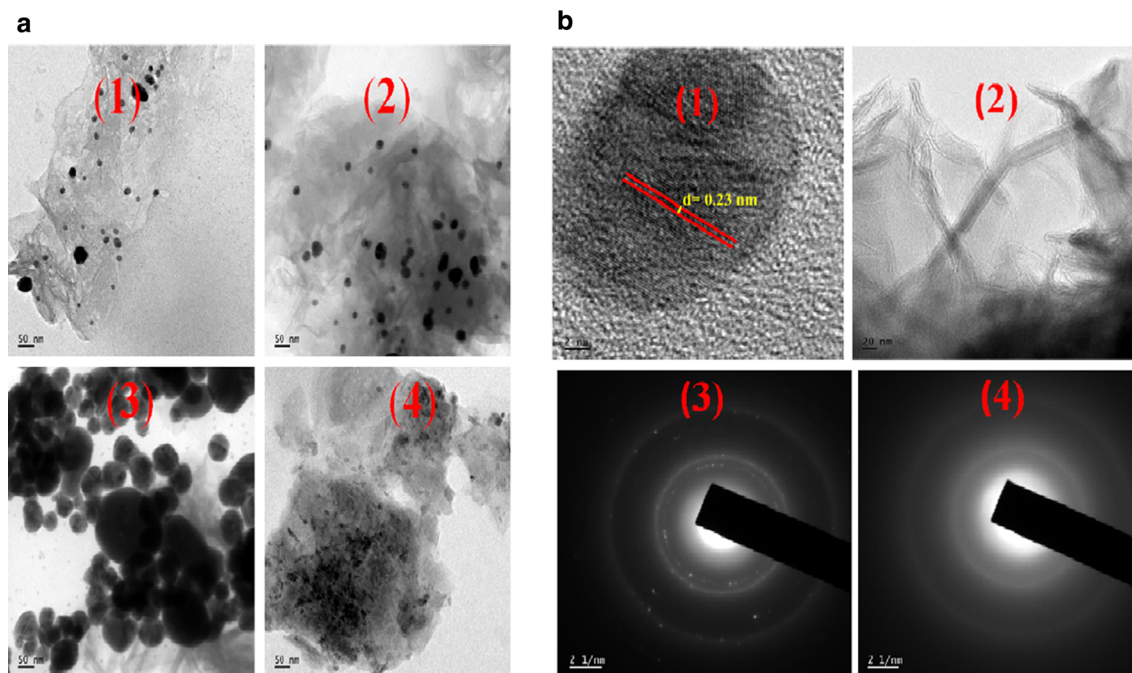


Fig. 7 **a** TEM image of NF-RGO/Ag hybrid at various concentrations of AgNO_3 solution; 1 0.1 M at 50 nm scale, 2 0.3 M at 50 nm scale, 3 0.5 M at 50 nm scale and 4 1 M at 50 nm scale. **b**, 1 HRTEM

of NF-RGO/Ag hybrid at 0.1 M of AgNO_3 at 2 nm scale, 2 TEM image of NF-RGO at 20 nm scale, 3 SAED of NF-RGO/Ag at 0.1 M of (AgNO_3) at 2 nm scale and 4 SAED of NF-RGO at 2 nm scale

GO and NF-RGO/Ag composite samples as they are carbon-based materials, while Cu is derived from Cu grid used to carry out the EDAX measurement (Fig. 8).

4 Photoluminescence quenching study

4.1 Photoluminescence results

The photoluminescence (PL) spectra of NF-RGO and NF-RGO/Ag at different concentration of AgNO_3 are shown in Fig. 9. The PL intensity of NF-RGO monotonically decreases with an increase in the concentration of AgNO_3 solution. The spectrum of NF-RGO (Fig. 9a) exhibits peaks at 377, 400 and 421 nm. At 0.1 M AgNO_3 solution (Fig. 9b) photoluminescence signals are observed at the same peak position like NF-RGO, 377, 386, 400, and 421 nm but with low intensity. At 0.3 M of AgNO_3 solution (Fig. 9c), peaks at 382, 400 and 421 nm are observed with an additional broad peak in the visible region at 511 nm but very low intensity. When 0.5 M AgNO_3 solution was used, two peaks at 382 and 400 nm are observed. The PL spectrum at 1 M AgNO_3 solution (Fig. 9) shows two peaks at 372 and 391 nm but with less intensity compared to the corresponding peaks observed in NF-RGO spectrum and a peak at 425 nm. The decrease in the PL intensity as the AgNO_3 concentration increase is attributed to the strong interaction between localized surface Plasmon resonances (LSPR) of Ag

nanoparticles and NF-RGO [35, 36]. Addition of 0.3 and 0.5 M AgNO_3 solution to NF-RGO resulted in the disappearance of the peak at 377 nm and hypsochromic shift of the peak at 386 nm in NF-RGO to 382 nm in the hybrid material. This blue-shift might be attributed to the Burstein–Moss effect. This indicates a dynamic transfer of electron or energy in the as prepared composite (NF-RGO/Ag hybrid) with NF-RGO and Ag-NPs acting as the donor and acceptor, respectively [37]. Similar observation has been reported by Wen et al. [15] in which graphene oxide transfers electron to Au nanocluster. The different spectrum obtained at 1 M AgNO_3 (inset of Fig. 9) compared to the other could be attributed to the significant aggregation of silver nanoparticles in the sample.

4.2 Investigation of the quenching mechanism

The PL quenching can be described by the following classic Stern–Volmer relationship [38],

$$\frac{F_0}{F} = 1 + K_{sv} [Q] \quad (1)$$

where F_0 and F are the fluorescence intensities before and after the addition of quencher, respectively. K_{sv} is called the quenching constant and $[Q]$ is the concentration of the quencher. As seen in Fig. 10, the PL spectra is fitted with Gaussian line profile and from this, the peak at 400 nm was found to be constant. Therefore, Stern–Volmer plot was done with 400 nm as the corresponding peak for 0.1, 0.3,

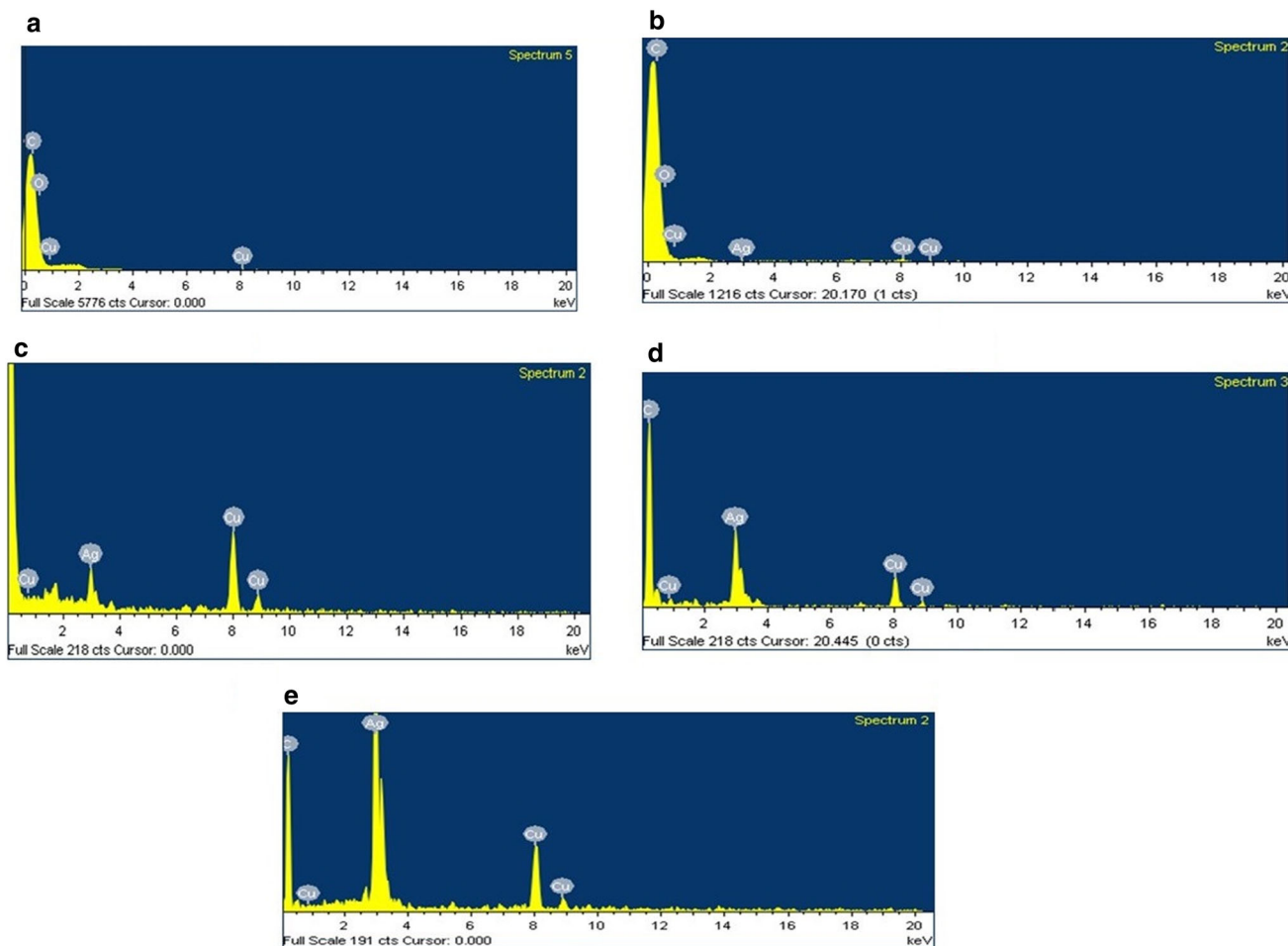


Fig. 8 EDS spectra of **a** GO and NF-RGO/Ag composite at various concentraions of AgNO₃ solution, **b** 0.1 M, **c** 0.3 M, **d** 0.5 M and **e** 1 M, respectively

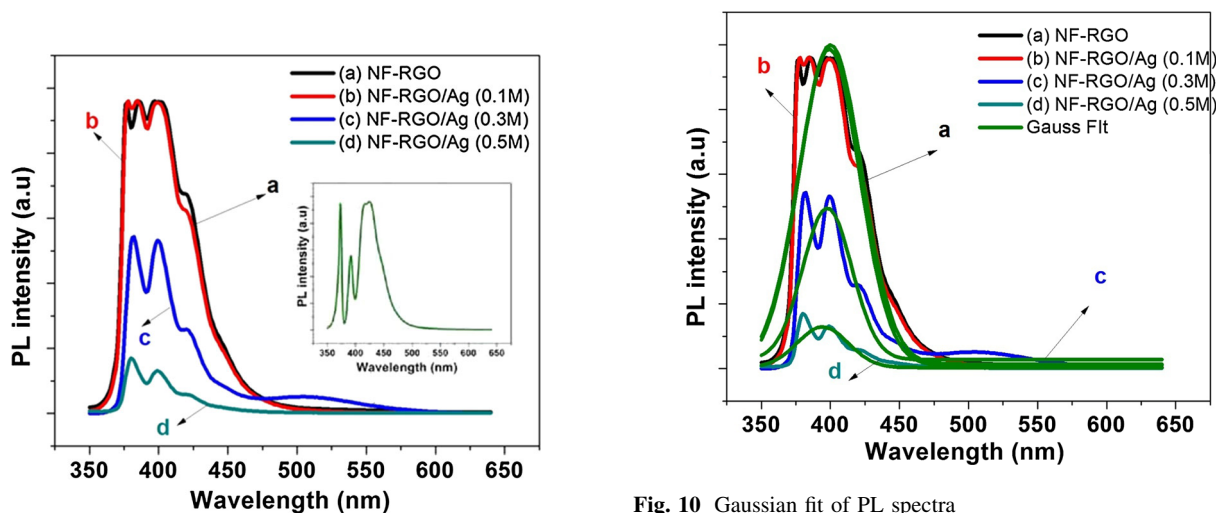


Fig. 9 Photoluminescence (PL) spectra of (a) NF-RGO and NF-RGO/Ag at various concentrations of AgNO₃ solution, (b) 0.1 M, (c) 0.3 M and (d) 0.5 M; inset Photoluminescence (PL) spectrum NF-RGO/Ag composite with 1 M concentration of AgNO₃

Fig. 10 Gaussian fit of PL spectra

and 0.5 M of AgNO₃ solution. As shown in Fig. 11, the standard Stern–Volmer plot was found to be nonlinear suggesting that both static and dynamic (energy or electron

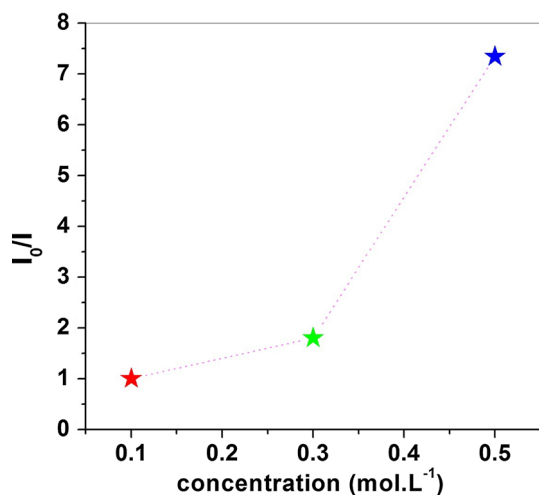


Fig. 11 Stern–Volmer plot

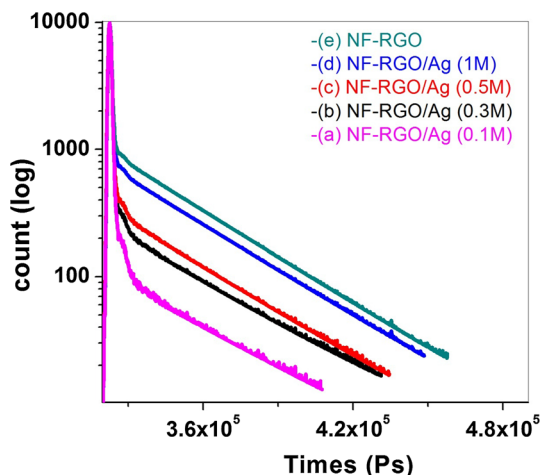


Fig. 12 Fluorescence decay curves of NF-RGO/Ag hybrid at various concentration of AgNO_3 solution, (a) 0.1 M, (b) 0.3 M, (c) 0.5 M and (d) 1 M and of (e) NF-RGO

transfer) quenching might be involved simultaneously in the quenching process, since more than one species are present in the as-synthesized hybrids [39–41]. Static quenching is through the formation of non-luminescent complex, while dynamic quenching can arise from energy transfer, electron transfer and non-luminescent exciplex formation. Thus, for better understanding of the quenching mechanism, life time measurement experiment was

performed. Samples were excited by a 340 nm pulsed diode light source with pulse duration less than one nanosecond. Figure 12 shows the fluorescence decay curves of NF-RGO and NF-RGO/Ag with different concentrations of AgNO_3 . The PL lifetime of the samples was determined by fitting the fluorescence decay curve perfectly with the following bi-exponential kinetics equation,

$$F(t) = A + B_1 \exp(-t/t_1) + B_2 \exp(-t/t_2) \quad (2)$$

The fitting parameters and average lifetime calculated using Eq. (3) are tabulated in Table 1.

$$\langle t_{Av} \rangle = \frac{\sum B_i \tau_i^2}{\sum B_i \tau_i} \quad (3)$$

PL lifetime was found to increase in the NF-RGO/Ag composite compared to the reference sample NF-RGO. In addition, the PL lifetime of NF-RGO/Ag hybrid increases with the decreasing concentration of AgNO_3 solution. This is because at low concentration of AgNO_3 , Ag-NPs are well dispersed and attached on the surface of NF-RGO but at high concentration of AgNO_3 , the as synthesized Ag-NPs aggregate. Therefore, the improvement of PL lifetime in the NF-RGO/Ag composite ruled out any possibility of static quenching or of dynamic non luminescent exciplex formation [40]. However, it confirms that there is a dynamic energy transfer from NF-RGO to Ag-NPs. This is in agreement with the blue-shift enumerated earlier in PL data analysis. In fact, the acceptor material (Ag-NPs) gained energy from the donor material (NF-RGO) to enhance its PL properties and consequently reduce the PL properties of its donor [42, 43].

5 Conclusion

A novel, simple and efficient two-step process for the synthesis of non-covalently functionalized reduced graphene oxide/silver nanoparticle hybrid (NF-RGO/Ag hybrid) is reported. Structural characterizations show that the averages particle sizes of Ag-NPs attached on the surface of NF-RGO increased with increasing AgNO_3 solution and tend to aggregate at high concentration of AgNO_3 . The results showed that 0.5 M is the optimum concentration under this reaction condition. The UV–Vis absorption spectroscopy analyses shows that the –COOH

Table 1 Fitting parameters of fluorescence decay curves performed by TCSPC technique

Samples	T_1 (ps)	T_2 (10^4 ps)	B_1	B_2	$\langle \tau_{av} \rangle 10^{-2}$ (ps)
NF-RGO	7.83	3.75	4,679,591	0.00175	6.74
NF-RGO/Ag (0.1 M)	4000	9.49	0.000725	320,113.9	949
NF-RGO/Ag (0.3 M)	8.48	3.54	1,392,656	0.00691	73.2
NF-RGO/Ag (0.5 M)	5.38	3.63	5.12×10^9	0.00240	14.8
NF-RGO/Ag (1 M)	7.57	3.61	7,913,799	0.00525	11.5

groups of PCA provide sites for hydrogen bonding with silver nanoparticle. Furthermore, the UV–Vis spectra show that, the SPR absorption band of Ag-NPs disappeared when 0.1 and 1 M of AgNO₃ were used. This might be attributed to the low Ag-NPs concentration at 0.1 M hence, no reduction reaction. At high concentration of 1 M, the rate of reduction is very slow due to insufficient reductant present in the solution. The EDAX data shows a decrease in oxygen content as the AgNO₃ concentration increased which suggests that the presence of Ag-NPs improved the structural restoration of GO. Due to the strong interaction between localized surface Plasmon resonances of Ag-NPs and NF-RGO, the PL intensity decreases with increase in concentration of the AgNO₃ concentration. The photo-physical investigations demonstrate that the nature of the photoluminescence quenching in NF-RGO/Ag hybrid is an unusual dynamic energy transfer with NF-RGO as the donor material. Understanding the PL quenching mechanism of NF-RGO/Ag-PNs hybrid is crucially important because materials with such properties could be used in energy conversion applications such as photovoltaic, photocatalysis and photochemical applications.

Acknowledgments Indian Council for Cultural Relations (ICCR—Govt. of India) is gratefully acknowledged for their financial and moral support. The authors would like to acknowledge the financial support from the Department of Science and Technology (DST—Govt. of India) through the Nano Mission, PURSE, FIST Programs and UGC—Govt. of India for the SAP Program. Financial support from the Ministry of Education of Republic of Senegal is also highly acknowledged.

References

1. K.S. Novoselov, A.K. Geim, S.V. Morozov, D. Jiang, Y. Zhang, S.V. Dubonos, I.V. Grigorieva, A.A. Firsov, *Science* **306**, 666 (2004)
2. X. Huang, X. Qi, F. Boey, H. Zhang, *Chem. Soc. Rev.* **41**, 666 (2012)
3. Y. Zhu, S. Murali, W. Cai, X. Li, J.W. Suk, J.R. Potts, R.S. Ruoff, *Adv. Mater.* **22**, 3906 (2010)
4. A.M. Zaniewski, M. Schriver, J. Gloria Lee, M.F. Crommie, A. Zettl, *Appl. Phys. Lett.* **102**, 023108 (2013)
5. F. Akbar, M. Kolahdouz, S. Larimian, B. Radfar, H.H. Radamson, *J. Mater. Sci. Mater. Electron.* **26**, 4347 (2015)
6. J.M. Urban, P. Dabrowski, J. Binder, M. Kopciuszynski, A. Wyszmołek, Z. Klusek, M. Jałochowski, W. Strupinski, J.M. Baranowski, *J. Appl. Phys.* **115**, 233504 (2014)
7. S. Murphy, L. Huang, P.V. Kamat, *J. Phys. Chem. C* **117**, 4740 (2013)
8. D.A. Dinh, K.S. Hui, K.N. Hui, Y.R.C.W. Zho, X. Hong, *Appl. Surf. Sci.* **298**, 62 (2014)
9. H. Bai, Y. Xu, L. Zhao, C. Li, G. Shi, *Chem. Commun.* **7**, 1667 (2009)
10. X. An, T. Simmons, R. Shah, C. Wolfe, K.M. Lewis, M. Washington, S.K. Nayak, S. Talapatra, S. Kar, *Nano Lett.* **10**, 4295 (2010)
11. Z. Chen, S. Berciaud, C. Nuckolls, T.F. Heinz, L.E. Brus, *ACS Nano* **4**, 2964 (2010)
12. M. Supur, K. Ohkubo, S. Fukuzumi, *Chem. Commun.* **50**, 13359 (2014)
13. M. Jiang, D. Zhu, H. Zhang, X. Zhao, *New J. Chem.* **38**, 3354 (2014)
14. M.E. Ragoussi, G. Katsukis, A. Roth, J. Malig, G. Torre, D.M. Guldi, T. Torres, *J. Am. Chem. Soc.* **136**, 14593 (2014)
15. X. Wen, P. Yu, Y.R. Toh, Y.C. Lee, K.Y. Huang, S. Huang, S. Shrestha, G. Conibeer, J. Tang, *J. Mater. Chem. C* **2**, 3826 (2014)
16. P. Routh, R.K. Layek, A.K. Nandi, *Carbon* **50**, 3422 (2012)
17. M.E. Khan, M.M. Khan, M.H. Cho, *New J. Chem.* **39**, 8121 (2015)
18. X.Z. Tang, Z. Cao, H.B. Zhang, J. Liu, Z.Z. Yu, *Chem. Commun.* **47**, 3084 (2011)
19. M.L. Yola, V.K. Gupta, T. Eren, A.E. Şen, N. Ata, *Electrochim. Acta* **120**, 204 (2014)
20. H. Mehl, M.M. Oliveira, A.J.G. Zarbin, *J. Colloid Interface Sci.* **438**, 29 (2015)
21. W.S. Hummers, R.E. Offeman, *ACS* **80**, 1339 (1958)
22. D.C. Marcano, D.V. Kosynkin, J.M. Berlin, A. Sinitskii, Z. Sun, A. Slesarev, L.B. Alemany, W. Lu, J.M. Tour, *ACS Nano* **4**, 4806 (2010)
23. K. Krishnamoorthy, M. Veerapandian, K. Yun, S.J. Kim, *Carbon* **53**, 38 (2013)
24. P.G. Ren, D.X. Yan, X. Ji, T. Chen, *Nanotechnology* **22**, 055705 (2011)
25. D. Parviz, S. Das, H.S.T. Ahmed, F. Irin, S. Bhattacharia, M.J. Green, *ACS Nano* **6**, 8857 (2012)
26. C. Xu, X. Wang, J. Zhu, *J. Phys. Chem. C* **112**, 19841 (2008)
27. P.K. Srivastava, S. Ghosh, *Appl. Phys. Lett.* **102**, 043102 (2013)
28. X. An, T.W. Butler, M. Washington, S.K. Nayak, S. Kar, *ACS Nano* **5**, 1003 (2011)
29. C.K. Chua, M. Pumera, *J. Mater. Chem. A* **1**, 1892 (2013)
30. W. Yuan, Y. Gu, L. Li, *Appl. Surf. Sci.* **261**, 753 (2012)
31. F. Liu, M.H. Jang, H.D. Ha, J.H. Kim, Y.H. Cho, *Adv. Mater.* **25**, 3657 (2013)
32. W. Ye, X. Shi, J. Su, Y. Chen, J. Fu, X. Zhao, F. Zhou, C. Wang, D. Xu, *Appl. Catal. B Environ.* **160–161**, 400 (2014)
33. Y. Zhou, X. Cheng, D. Du, J. Yang, N. Zhao, S. Ma, T. Zhong, Y. Lin, *J. Mater. Chem. C* **2**, 6850 (2014)
34. M.R. Das, R.K. Sarma, R. Saikia, V.S. Kalec, M.V. Shelke, P. Sengupta, *Colloids Surf. B Biointerfaces* **83**, 16 (2011)
35. O.A. Balitskii, M. Sytnyk, J. Stangl, D. Primetzhofer, H. Groiss, W. Heiss, A.C.S. *Appl. Mater. Interfaces* **6**, 17770 (2014)
36. P. Reineck, D. Gómez, S.H. Ng, M. Karg, T. Bell, P. Mulvaney, U. Bach, *ACS Nano* **7**, 6636 (2013)
37. J. Yang, X. Zhao, X. Shan, H. Fan, L. Yang, Y. Zhang, X. Li, *J. Alloys Compd.* **556**, 1 (2013)
38. F. Wang, Z. Gu, W. Lei, W. Wang, X. Xia, Q. Hao, *Sens. Actuators B* **190**, 516 (2014)
39. C. Baslak, M. Kus, Y. Cengeloglu, M. Ersoz, *J. Lumin.* **153**, 177 (2014)
40. J. Keizer, *J. Am. Chem. Soc.* **105**, 1494 (1983)
41. P.J. Goutam, D.K. Singh, P.K. Iyer, *J. Phys. Chem. C* **116**, 8196 (2012)
42. F. Yang, W. An, W. Zhuang, G.S. Tian, X.P. Jing, *J. Lumin.* **146**, 269 (2014)
43. T. He, R. Che, Z.B. Lim, D. Rajwar, L. Ma, Y. Wang, Y. Gao, A.C. Grimsdale, H. Sun, *Adv. Opt. Mater.* **2**, 40 (2014)